

COVER PAGE

Document downloaded by @DAEL

Thu Nov 26 14:50:18 2026
For personal use

When automatic English translation is provided, only the original document is authentic.
The EAA cannot be held responsible of any translation error

Bibliographical reference

The Bow on a String: Bow Vibrations Detected with Ferroelectret Sensors, Gunnar Gidion and Reimund Gerhard, Acta Acustica **vol. 104** (Number 2), 2018, pp. 315-322

DOI
https://doi.org/10.3813/AAA.919174

Acta Acustica united with Acustica
Vol. 104 (2018) 315 – 322

DOI 10.3813/AAA.919174

The Bow on a String: Bow Vibrations Detected with Ferroelectret Sensors

Gunnar Gidion, Reimund Gerhard
Applied Condensed-Matter Physics, Institute of Physics and Astronomy, University of Potsdam, 14476 Potsdam, Germany. gidion@uni-potsdam.de

Summary
The interaction between a bowed string instrument and its player is conveyed by the bow, the vibrational properties of which can be measured either separately on the bow or during the bowing procedure. Here, two piezoelectric film sensors, made of a ferroelectret material, are installed on a violin bow, one sensor at the tip and one at the frog. With these sensors, a violin is played under normal conditions, and the signals are analysed. The features in the resulting spectrograms are identified as string harmonics and longitudinal bow-hair resonances. The bow-hair sections on both sides of the bow-string contact exhibit separate resonances which are observed as absorption dips in the spectra. Owing to the sensor positions at the bow-hair terminations, it can be inferred that the two bow-hair sections act as mutual vibration absorbers. From a regression of the observed resonances, the longitudinal bow-hair velocity can be obtained. With additional film sensors under the violin bridge, body vibrations were also detected providing further details of the coupling mechanisms.

PACS no. 43.75.De, 43.38.Fx, 43.38.-p, 43.75.Yy, 43.75.-z

1. Introduction

For a player of a bowed string instrument, the bow is part of the feedback loop for controlling the sound radiated from the instrument. The predominant input to the player is the audible sound, but there is also haptic feedback, as bow vibrations can be sensed by the hand that is operating the bow. If and how this haptic information is used to adjust the handling of the bow, remains an open question. In any case, it is instructive to touch the bow hair while bowing a string: The tickling that can be felt provides a clear evidence that the bow is excited by the bow-string interaction.

Thus, for a comprehensive description of the bow-string interaction, the elastic compliance of the bow hair has to be taken into account. Any yielding or vibrations of the bow hair, which are always associated with elastic deformations of the rest of the bow, may influence the string vibrations. In this way, the bow vibrations might contribute to the perceived sound. The bow-string energy transfer in both directions will only be significant, if the characteristic impedances of bow and string are of comparable magnitude. There has been an ongoing discussion about this since the seminal paper by Schumacher [1] in 1975, and significant results about the dynamic properties of the bow have been published in the meantime, see *e.g.* references [2, 3, 4, 5].

Received 10 July 2017,
accepted 15 January 2018.

By installing piezoelectric film sensors on a violin bow and under the violin bridge, we were able to observe some vibrational features of the bow during playing, features that are related to the string-bow and bow-instrument interactions. Before the results are described, analysed and discussed, several known vibrational properties of the bow are summarised. Moreover, the application of sensors on the bow for the detection of bowing parameters is briefly reviewed.

1.1. Bow modes and bowing parameters

Probably the most obvious bow modes, especially for the player, are the bouncing modes when the bow is perched on the string (or any other edge-like structure). The bouncing frequencies range from 6 to 30 Hz, depending on the position x of the string on the bow, with lower frequencies nearer to the frog. The observed modes involve hair and stick vibrations (both transverse to the bow axis), with the bow acting as mass and spring, and are weakly dependent on the bow-hair tension. Their excitation can be detrimental to the sound during normal "detaché" bowing, but the bouncing is also exploited for faster bowing techniques [6, 3].

Askenfelt [2] pointed out that the coupling between the taut bow hair and the stick makes it hard to clearly distinguish separate modes of either subsystem. With this reservation, in admittance measurements with excitation and motion detection perpendicular to the bow hair ("transversal admittance"), he identified transverse bow-hair modes in the range below 500 Hz. The fundamental stick mode

© S. Hirzel Verlag · EAA

Document downloaded by @DAEL, 2026-11-26 14:50:23 - personal use only

and the fundamental transverse bow-hair mode have resonance frequencies of about 60 Hz. Gough [3] showed that the coupling of these modes can lead to a "veering and splitting" of resonances, similar to the related phenomena on coupled strings [7, 8].

With respect to the longitudinal bow admittance (parallel to the bow hair), however, Askenfelt assigned most of the resonance peaks below 3 kHz to stick modes. In addition, he related two peaks, at 1.6 kHz and below 6 kHz, respectively, to the first and third longitudinal bow-hair modes. The second mode was missing in the spectra because admittance was measured at the midpoint of the bow-hair ribbon. The interpretation of the admittance measurements was confirmed in general by Gough's simulations [3].

The player's hand was found to have an influence on the bow modes insofar, as it introduced strong damping. But the resonance frequencies were not changed significantly [9, 3].

Sensing devices (accelerometers, force sensors and microphones) on the bow have not only been used to investigate the properties of the bow itself (as in the investigations described above), but also to measure the bow force during playing [10, 11, 12, 13, 14, 15]. The bow force is one of the parameters through which the dynamic regime of the string is controlled. The other most relevant parameters are bow velocity and bow-bridge distance. Ever since Raman first investigated the conditions for Helmholtz-type motion on the bowed string [16], the process has been a matter of interest. The parameter limits for Helmholtz motion have been examined theoretically [17, 18] and numerically [19, 20], but were also determined experimentally [10, 14, 21, 22]. The capture of bow force is also essential for studies of bowing technique in general [12, 13, 15]. Two types of experiments can be distinguished: Either a bowing machine is used to systematically control the bowing parameters, or a real bow is equipped with sensors. Demoucron *et al.*, for example, have documented the thorough calibration of a system with strain gauges on the bow (based on Askenfelt's configuration [10]) for measuring the bow force during playing [11].

The piezoelectric polymer-film sensors that we employ here had originally been designed to measure bow force. However, it turned out that the high-frequency components of the recorded signals also contained features related to instrument-bow coupling, which we try to show in this paper.

2. Experiments

2.1. Ferroelectret transducers

In addition to classical piezoelectric crystals and ceramics, other types of materials exist which exhibit a piezoelectric effect. Examples are soft-matter functional materials — polymers that contain dipoles either as dipole molecules or as fixed space charges of both polarities. The compression of such samples either leads to a shrinking of the polymer matrix in which the molecular dipoles are embedded, or the dipoles themselves change their dimensions. In both cases, the electrode charges must change as well. For a general model of piezoelectricity which incorporates all possible mechanisms, see [23, 24]. Piezoelectric polymer-film sensors have already been used for measuring organ-pipe wall vibrations [25], resonances of piano soundboards during different construction phases [26], and violin-bridge vibrations [27]. The same type of film sensors as in [27], made from piezoelectric poly(vinylidene fluoride) or PVDF, was also used here to compare the bridge-body vibrations of the violin with the simultaneous bow vibrations.

The film sensors employed here for the detection of bow dynamics were made from cellular-polypropylene (PP) foam, with a thickness of about 70 μm; the preparation process is described in [28]. In piezoelectric PP, which is a soft foam, charges at the inner surfaces of the foam cavities form permanent electric dipoles, the moments of which are changed by compression. The term "ferroelectret" has been introduced for this material because of hysteresis behaviour during poling cycles that is essentially analogous to a ferromagnetic hysteresis [29].

Piezoelectric films are used as transducers with a top and a bottom electrode. The electrodes are very thin metal layers (< 50 nm) that are typically deposited by vacuum evaporation. Any charges that are generated within the area of the electrodes can be detected. For the present investigations, a Brüel & Kjær Nexus charge amplifier type 2692 was used to amplify the sensor signals, which were subsequently recorded by means of a soundcard and a computer.

One film sensor was installed at the tip of the bow between the bow-hair ribbon and the small plate at the tip. Another sensor was held between an additionally mounted acrylic block and the bow hair near the frog, see Figure 1b and 1a, respectively. As can also be seen in the photographs, cables were used to connect the sensors to the amplifier. The cable from the tip was fixed to the bow stick, so that both cables were dangling from the frog-end of the bow during playing. The sensitivities of the sensors at tip and frog were $d_{33} = 166$ pC/N and $d_{33} = 129$ pC/N, respectively, where d_{33} is the piezoelectric coefficient for the case that both mechanical stress and resulting electrical field are in the thickness (3) direction. Therefore, with the sensitivity described by the d_{33} coefficients, any transverse motions of the bow-hair ribbon and the associated bow-stick deformations are captured. In principle, piezoelectric polymer films are also sensitive to shear deformations, but this property is not well investigated for ferroelectrets. So any slight shear deformations that could appear in the present configuration of film sensors on the bow, cannot be assessed in terms of contribution to sensor output.

2.2. Bowing procedure

A succession of a down- and an up-bow stroke was performed on a violin, involving one intermittent bow change (change of direction of motion). It was attempted to keep

Document downloaded by @DAEL, 2026-11-26 14:50:23 - personal use only

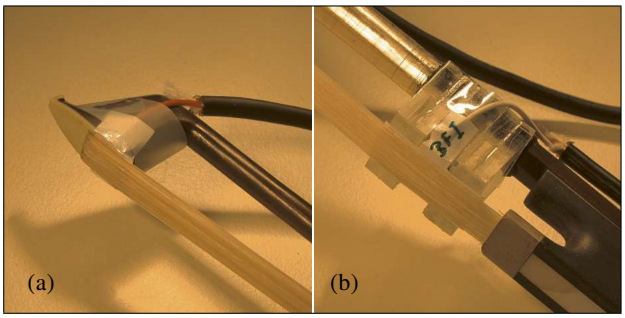


Figure 1. Film sensors on a violin bow, fixed by bow-hair tension at the tip (a), and near the frog (b) with a specifically designed mounting support.

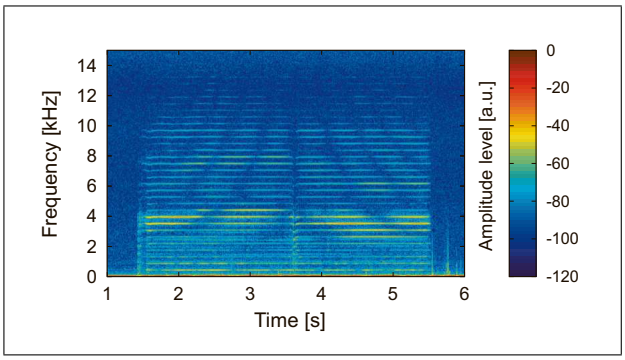


Figure 2. Spectrogram obtained with the sensor at the frog during down- and upbow on an A string.

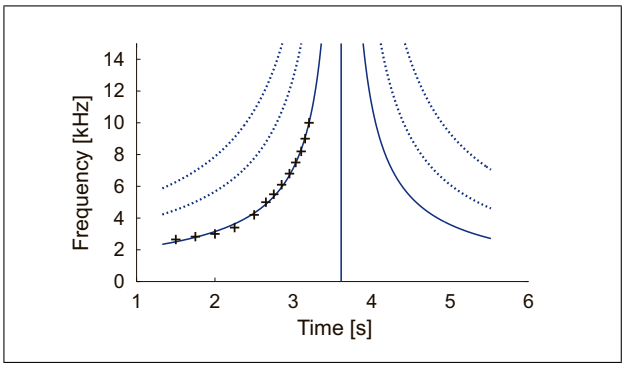


Figure 3. Regression curves to the patterns in the spectrogram of the frog-sensor signal (Figure 2). The vertical line at $t = 3.7$ s seperates the down-bow from the subsequent up-bow stroke. Here – for the frog sensor – plus signs mark the points that have been picked for the down-bow regression. The curves for the higher modes (dotted lines) are simply obtained by appropriate multiplication of the fundamental curve.

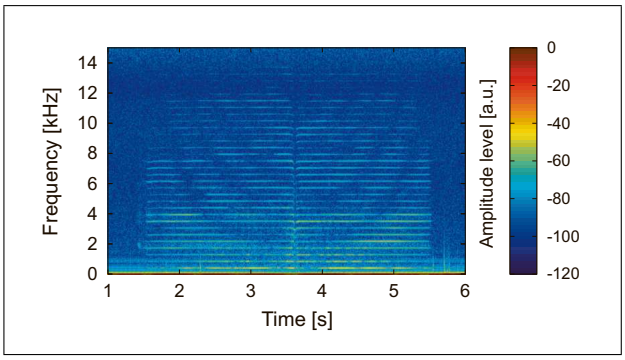


Figure 4. Spectrogram obtained with the sensor at the tip during down- and upbow on an A string.

bow force and speed constant during bowing. The bow-hair tension was kept constant by adjusting the minimum hair-stick distance to 9.7 mm. However, the actual hair tension depends on the properties of the bow [30]. The player also tried to maintain a constant bow-bridge distance of $d_{bb} \approx 2.5$ cm, which is an intermediate position between the bridge and the fingerboard. With a violin-string length of 32.5 cm, this corresponds to a relative bow-bridge distance of $\beta \approx 0.08$.

Furthermore, almost the entire length of the available bow hair ($l = 61$ cm, due to a length reduction by the sensor block, Figure 1b) was used for each stroke. It takes some practice to get used to the cabling, and the sensor mount near the frog also adds an unfamiliar feel, but after some training, a satisfactory sound can be produced. Signals from both sensors on the bow were recorded simultaneously. In addition, the motion of the bridge feet was recorded with PVDF film sensors installed between the bass and treble foot and the top plate, respectively (as described in [27]).

From the signals, spectrograms were calculated, cf. Figures 2 (sensor at the frog) and 4 (sensor at the tip), where the results obtained during the down-up bow cycle on an A string are shown.

In addition, the FFT spectra of the down- and upbow intervals, are depicted in Figure 6 and complemented with the FFTs of the measurements at the bridge feet.

A linear scale is chosen to accentuate differences.

The results from bowing an open A string are used as an example. But the basic features that are observed and discussed below also appear when other strings are bowed.

3. Observations

At first glance, the horizontal lines in the spectrograms of the bow-sensor signals (Figures 2 and 4) show that string harmonics (440 Hz and multiples) are detected at the bow hair terminations. This also becomes obvious in the FFT spectra shown in Figure 6 which are discussed below. Although the amplitudes become quite low at higher frequencies, harmonics up to almost 14 kHz can be identified in the spectrograms, corresponding approximately to the 30th harmonic. From the onset of these lines, it can be inferred that the down-bow is started at $t_i = 1.5$ s. The bow change takes place at the short interruption of the lines at $t_f = 3.7$ s and the up-bow ends at 5.5 s.

The horizontal lines of the string harmonics in Figures 2 and 4 are intersected by resonance-like patterns or trends that change with the position x of the string on the bow (or the bow position (according to [10]), as measured from the frog, see Figure 7). Interestingly, these trends are minima in the spectrograms and also occur as a family of modes.

Document downloaded by @DAEL, 2026-11-26 14:50:23 - personal use only

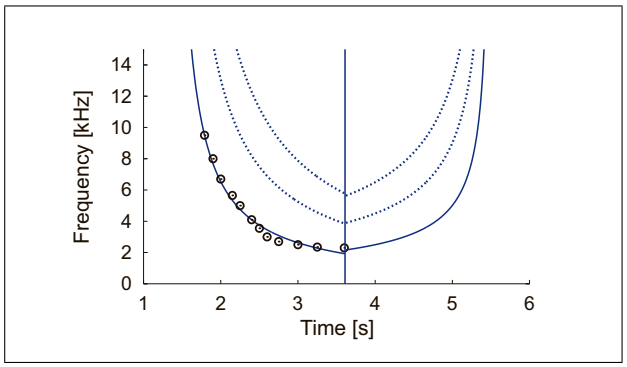


Figure 5. Regression curves to the patterns in the spectrogram of the tip-sensor signal (Figure 4), analogous to Figure 3 for the frog sensor. In this case, *i.e.* for the tip sensor, the points chosen for the regression are marked by circles.

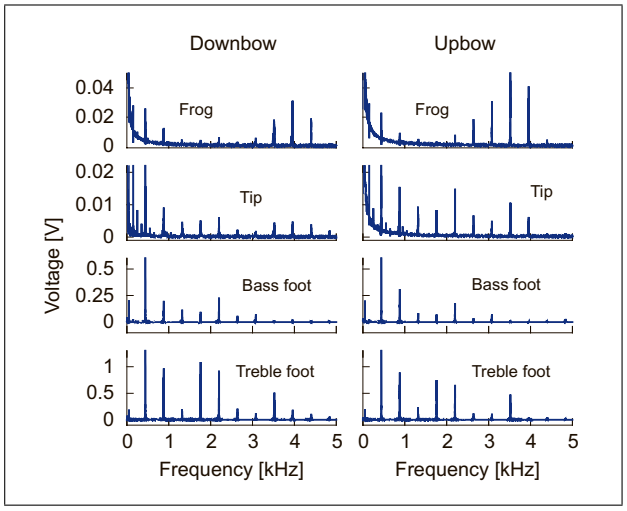


Figure 6. FFT spectra of down- and upbow with sensors on the bow (tip and frog), as shown in the spectrograms of Figures 2 and 4. In the four lower spectra, the signals of two film sensors under the bridge feet (bass and treble) are evaluated.

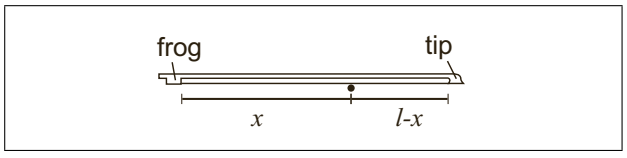


Figure 7. Division of the bow-hair ribbon by the string into two sections. Any deflections due to bow force are neglected here (for their description, see [30]).

The patterns produced in this way may be relatively weak, but they are consistently observed for all strings.

Points on the trends in the spectrograms were arbitrarily selected for a subsequent regression analysis which will be described in the following section. In Figures 3 and 5, the calculated regression curves are plotted for the frog- and tip-sensor spectrograms, respectively, together with the selected points from the down-bow stroke. The sensor position is indicated either by a plus sign for the frog sensor or by a circle for the tip sensor. In the following, the down-bow stroke will serve as an example for the regression analysis. The curves for higher (bow or bow-hair) modes that are also plotted in Figures 3 and 5 have not been obtained from a regression, but are approximate multiples of the fundamental trends.

The observed patterns are symmetrical with regard to the bowing direction, which means that the time t_f of the bow change is the center of symmetry. Thus, the pattern obtained from the tip sensor looks like a menorah (cf. Figure 5), whereas the curves from the frog sensor resemble a volcano (Figure 3).

To be more specific, during the down-bow, trends with increasing frequencies can be seen in the spectrogram obtained at the frog, whereas at the tip for the same interval, trends with decreasing frequencies are generated. It should also be noted that both features, the string vibrations as well as the trends, can be *heard* when the respective recordings are played back. The bowed-string sound is perceived quite clearly, but it appears modulated by a filter that changes with time.

An additional feature that stands out in the spectrograms of the bow sensors is the higher intensity of harmonics between 3 and 4 kHz. This can be seen in more detail in the FFT spectra of Figure 6. The bow vibrations during the down-bow have a broad peak spreading from the eighth to the tenth harmonic (with a maximum at the ninth at 3.96 kHz). In contrast, during the upbow, the eighth harmonic (3.52 kHz) is a maximum in the bow vibrations and also the treble foot vibrations.

Furthermore, at frequencies below 440 Hz, no further systematic features could be observed in the spectra, which is not surprising because the string harmonics provide the main excitation frequencies here. However, there is a weak contribution at lower frequencies by the mains hum at 50 Hz and multiples that can be spotted in the intervals before the down-bow and after the up-bow stroke in Figures 2 and 4.

4. Analysis

The trends observed in the spectrograms obviously depend on the bow position x (cf. Figure 7). The parameter has not been determined, but under the assumption of constant bow velocity, the bow position x depends linearly on time, *e.g.*, for the down-bow:

$$x(t) = \frac{t - t_i}{t_f - t_i} \cdot l, \tag{1}$$

where t_i is again the onset of bowing and t_f is the time of the bow change, or rather, the end of the down-bow stroke.

If we assume that resonances of the two bow-hair sections adjacent to the string, with lengths x and $l-x$, respectively (cf. Figure 7), are the cause of the observed trends, we may simply model the resonance frequencies as being proportional to the reciprocals of these lengths as expected for a half-wavelength (or string-like) resonator. Thus, for the dependence on the bow position during the down-bow stroke, we can write

$$f_{\mathrm{bow,o}} = \frac{c}{2} x^{-1} \tag{2}$$

Document downloaded by @DAEL, 2026-11-26 14:50:23 - personal use only

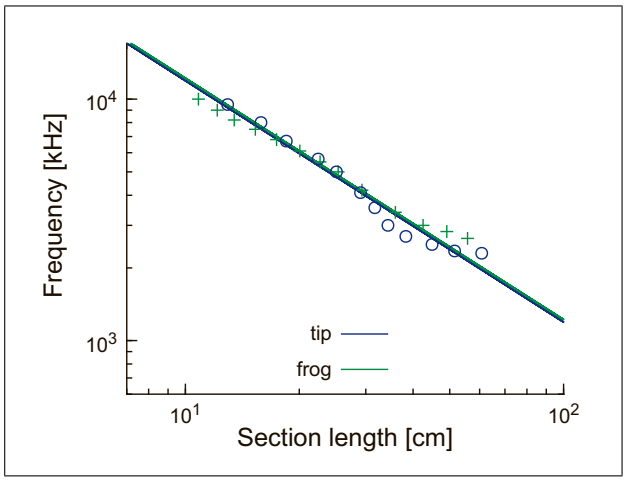


Figure 8. Linear regression in a log-log plot of the frequencies found in spectrograms of vibrations detected at the tip (∘) and at the frog (+), as shown in Figures 2 and 4, versus the assumed resonating lengths of the bow-hair sections.

for the sensor at the tip (decreasing frequencies) and

$$f_{\mathrm{bow},+} = \frac{c}{2}\left(l - x\right)^{-1} \tag{3}$$

for the sensor at the frog, respectively. The constant c in these equations is the wave velocity on the bow hair. It can be determined from the fits of the functions (2) and (3) to the arbitrarily selected points on the trends observed in Figures 2 and 4.

The fit parameters were obtained from a linear regression of the logarithms of the resonance frequencies f_{bow} and the section lengths x (for the tip), or $l - x$ (for the frog):

$$\log \frac{f_{\mathrm{bow},\circ}}{f_0} = \log\left(\frac{c}{2c_0} \cdot \frac{x_0}{x}\right) \tag{4}$$

$$= \log \frac{c}{2c_0} - \log \frac{x}{x_0} \tag{5}$$

and

$$\log \frac{f_{\mathrm{bow},+}}{f_0} = \log \frac{c}{2c_0} - \log \frac{l-x}{x_0}. \tag{6}$$

The reference values $f_0 = c_0/x_0 = 1/\mathrm{s}$, $c_0 = 1\mathrm{m/s}$ and $x_0 = 1\mathrm{m}$ have been introduced to facilitate the calculation of the logarithms.

With the slopes fixed at -1, the y-intercept

$$a = \log \frac{c}{2c_0} \tag{7}$$

is the only variable determined from the regressions. The log-log plot of the frequencies f_{bow} in Figure 8 illustrates the procedure. Linear regressions are obtained for both signals separately, from the tip and the frog, respectively. We obtain wave velocities according to the relation

$$c(a) = 2c_0 \cdot 10^a, \tag{8}$$

Table I. Wave velocities c obtained from linear regressions in log-log plot (according to eqs. (4)-(6)) of the observed trends, with slope fixed at -1. In addition, the slopes determined from regressions with variable slope are given.

String	Sensor	Stroke	c [km/s]	Slope
G	tip	down	2.83 ± 0.03	-0.99
		up	2.2 ± 0.2	-0.79
	frog	down	1.8 ± 0.4	-0.51
		up	1.8 ± 0.5	-0.46
D	tip	down	2.66 ± 0.04	-0.97
		up	2.2 ± 0.2	-0.75
	frog	down	2.4 ± 0.2	-0.79
		up	2.4 ± 0.2	-0.76
A	tip	down	2.9 ± 0.1	-0.87
		up	2.2 ± 0.2	-0.71
	frog	down	2.0 ± 0.2	-0.68
		up	2.38 ± 0.01	-0.77
E	tip	down	2.6 ± 0.2	-0.76
		up	2.1 ± 0.2	-0.73
	frog	down	2.0 ± 0.2	-0.64
		up	2.4 ± 0.2	-0.79

which results from equation (7). For the depicted example (down-bow on a violin A string), this procedure yields wave velocities $c = (2.4 \pm 0.3)\,\mathrm{km/s}$ for the signal recorded at the frog, and $(2.4 \pm 0.2)\,\mathrm{km/s}$ for the tip signal. The given standard deviations result from the standard deviations Δa of the linear regressions by also taking into account the propagation of uncertainty (in linear approximation): $\Delta c \approx \partial c/\partial a \cdot \Delta a = 2c_0 \ln a \cdot 10^a \cdot \Delta a$. It is also important to note that regressions with variable slope yield slopes of -0.84 for the frog-sensor spectrogram and of -1.00 for the sensor at the tip.

With another violin, but using the same bow, the experiments and evaluation as described above were again performed for all open strings and for both bowing directions. The results are given in Table I.

5. Discussion

The string harmonics that are detected at the bow-hair terminations seem to be readily explainable as the result of forced vibrations. The stick-slip interaction that is associated with the Helmholtz motion of the string also generates longitudinal and transverse stresses of the bow hair. As the sensors mainly detect vibrations in their thickness direction, the transverse stresses of the bow hair should be the main reason for the detected string harmonics.

The resonance-like trends that are found as minima in the recorded spectra, interrupting the observed string harmonics, have already been shown to depend on the position x of the string on the bow. That is why the observed curves are probably due to resonances of the two sections into which the ribbon is divided by the string, with lengths l and $l - x$, respectively (cf. Figure 7). In this case, the

Document downloaded by @DAEL, 2026-11-26 14:50:23 - personal use only

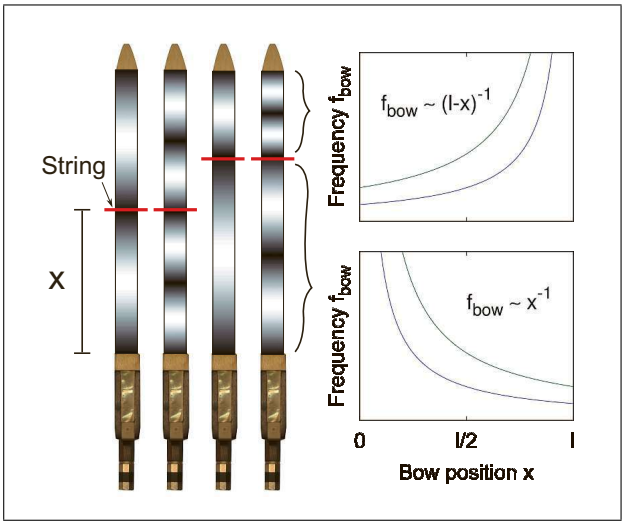


Figure 9. Schematic representation of the observed longitudinal bow-hair modes. The two lowest modes are shown on the left-hand side for bow positions $x = 0.5l$ and $x = 0.7l$. Right-hand side: The resonance frequencies of the two bow-hair sections change continuously with the bow position x according to the respective lengths x and $l - x$.

string provides a vibrational node which is plausible at least during the sticking phase. The resulting longitudinal standing waves are illustrated in Figure 9 together with the associated hyperbolic relation between the resonance frequencies and the bow position. The fact that the higher modes of these longitudinal waves do not appear as exact harmonics in most of the observed patterns, has to be ascribed to coupling to the elastic bow stick as well as to a relatively high damping in the bow hair ribbon. The damping also becomes apparent in the width of the curves.

That we observe minima, rather than resonance peaks, suggests some sort of dynamic absorption mechanism. This is further confirmed by the observation that, *e.g.*, the detected trend is not decreasing but increasing in frequency at the frog during the down-bow (Figure 2), although the length of the adjacent bow-hair section x is increasing.

Obviously, the two bow-hair sections act as mutual vibration absorbers: Some of the vibration energy that is produced by the bow-string interaction is transferred to the resonating section between string and tip, if the frequencies match, so that at the frog this portion of the spectrum is attenuated. The seeming inconsistency becomes apparent when comparing the behaviour of the longitudinal standing waves illustrated in Figure 9 with the trends in the measurements shown in Figures 2 and 4.

There is one severe objection, however, that could be made against the claim that the observed trends are due to mechanical absorption: Why do the resonances that lead to absorption not appear as maxima in the respective spectrogram of the opposite sensor? Two answers can be given.

First, there are some obvious, but rather blurry amplitude modulations of the string-resonance maxima in the spectrograms. These modulations might be related to the bow-hair resonances, but are not clear enough to be identified. It should be stressed again, too, that only forced bow vibrations are observed during playing, with excitation frequencies corresponding almost exclusively to string harmonics. Consequently, continuous trends of the described bow-hair resonances cannot be expected. Accordingly, the trends that appear due to the absorption are not continued between the string harmonics, either.

Second, longitudinal vibrations are hardly detected by the sensors and therefore the string harmonics which appear in the spectra are mainly due to transverse bow-hair vibrations. Therefore, the minima due to absorption are seen, while the associated longitudinal resonances, causing the absorption, remain hidden.

The fundamental frequencies of the longitudinal bow-hair modes that have been reported so far, lie between 1500 and 2000 Hz [2, 31, 1]. This corresponds to the lowest frequencies of the observed trends (for either $x = l$ or $x = 0$, depending on the sensor position). In the present case, these frequencies are a little bit above 2 kHz, maybe because the mounting of the sensor at the frog (Figure 1 (b)) shortens the effective bow-hair length. The chosen bow-hair tension, however, is not expected to have an influence on the resonance frequencies, according to [2].[1]

The wave velocities that are obtained by the linear regression to the trends are also in good agreement with longitudinal wave velocities that have been determined by different means. For example, Schumacher obtained $c_L = 2500\,\text{m/s} \pm 18\%$, by measuring the time of flight of impulses [5, 1]. Askenfelt also investigated longitudinal bow-hair modes and obtained velocities "in the range 2200–2400 m/s" [2].

The regressions of the up- and down-bow measurements on all four open strings shown in Table I yield an average longitudinal velocity of $\overline{c_L} = (2.3 \pm 0.3)$ km/s.[2] However, the resulting velocity obviously depends on the bowing direction as well as on the sensor position. In particular, the highest velocities are found for the sensor at the tip in combination with the down-bow stroke, on average $\overline{c_L} = (2.7 \pm 0.2)$ km/s. In comparison, the up-bow strokes yield $\overline{c_L} = (2.17 \pm 0.04)$ km/s at the tip. For the sensor at the frog, it is the other way around: Velocities are lower for the down-bow, namely $\overline{c_L} = (2.0 \pm 0.2)$ km/s, compared with $\overline{c_L} = (2.2 \pm 0.3)$ km/s for the up-bow. Although it is tempting, these deviations cannot be explained by the Doppler effect because it is too small for the present bow velocities.

Rather, we propose that systematic variations of the bow velocity are the reason for the observed differences. For the calculation of the bow position $x = x(t)$ according to equation (1), a constant bow velocity is assumed, which results in the linear relation. Thus, any deviations from a

[1] This was further confirmed in a measurement of the impulse response of the seperate bow recorded with the film sensor at the frog: An increase of the bow-hair tension mainly reduced the width of the longitudinal resonance peak.

[2] Here, and in the following, the mean of the respective data set and the corresponding standard deviations are given.

Document downloaded by @DAEL, 2026-11-26 14:50:23 - personal use only

constant bow velocity will result in an incorrect longitudinal velocity c_L because c_L is obtained from a regression with respect to the bow position x. In the present case, a systematic increase of the bow velocity during each stroke would indeed explain the observed deviations, especially as they are inverse with respect to sensor position and bowing direction. It would also account for the differences in slope (cf. Table I), if the slope is a free variable in the linear regression.

The relevance of the longitudinal wave velocity c_L on the bow hair can be seen from the following relations. It is directly related to the input impedance Z_L for longitudinal waves as well as to the elastic modulus E [32]:

$$Z_L = m' c_L = S\sqrt{E\rho}, \tag{9}$$

with the linear mass density $m' = \rho S$ of the bow-hair ribbon with cross section S (depending on the number of bow hairs taken into account, cf. [5]). The longitudinal input impedance of the bow hair, on the other hand, is the most relevant quantity for the assessment of the bow-string vibration transfer.

It has been argued and shown [2] that the bow-string coupling is facilitated if the bow-bridge distance coincides with the node of a string mode because this increases the string impedance. Around the resonance frequency of the respective mode, the bow is excited most during playing. This might explain the observed amplification in the bow spectra in Figure 6 between 3 and 4 kHz. If we allow the assumed bow-bridge distance $d_{bb} \approx 2.5$ cm to deviate by about a centimetre, $d_{bb} \approx 3.6$ cm, the relative bow-bridge distance is $\beta \approx 0.11$, making the ninth harmonic at 3.96 kHz the affected mode (with a string length of 32.5 cm). As described above, there is indeed a maximum of bow vibrations around that frequency, most pronounced at the frog. Another interpretation of the observed broad maximum of bow-vibration amplitudes around 4 kHz is the influence of Schelleng ripples (cf. [31, 17]), which occur with a frequency of $f_{ripples} = f_0/\beta = 440\,\text{Hz}/0.11 = 4\,\text{kHz}$, coincidentally also with assumed relative bow-bridge distance of $\beta = 0.11$. The analysis of further measurements not presented here seems to confirm the hypothesis of Schelleng ripples, but because of the possible concurrence of several phenomena (Schelleng ripples of transverse and torsional waves, bridge hill, torsional waves) a conclusive interpretation will not be attempted at this stage.

6. Conclusion

By means of two piezoelectric film sensors on a violin bow at the terminations of the bow hair, the transfer of string vibrations to the bow was observed. In time-resolved spectra of the two sensor signals, the bowed-string harmonics could be clearly identified. Moreover, additional trends were detected in the spectrograms that are interpreted as longitudinal bow-hair modes. These modes depend on the bow position, with the string defining a node of the bow-hair vibrations. These resonances are not detected as spectral maxima (as one might expect), but as minima of the film sensor-sensor signals, which mainly reveal transverse hair vibrations. This behaviour can be explained with an absorption mechanism: Whenever the longitudinal bow-hair resonance of one of the sections matches with the string harmonics, less vibration energy is transferred to the other section, which results in an absorption dip in the respective spectra. Simple regressions to the observed trends yielded longitudinal bow-hair wave velocities that agree well with the results of earlier investigations which have been conducted on bows at rest.

The actual maxima of bow vibrations as excited by the A string were found between 3 and 4 kHz. For the bow-string interaction in general, not only the respective impedances play a role, but also the bow-bridge distance which might influence the observed bow-vibration maxima most, *e.g.* with respect to Schelleng ripples.

In the end, the coupling strength as well as the excitation of modes depend on the actually played note. Thus, for every bowed note, not only the instrument but also the bow will show a different behaviour. This makes the scientific assessment even more difficult and it also poses a challenge to the player. Although it still seems an open question what the player is able to perceive with his bowing hand and exploit for the playing, some of the bow dynamics observed here may well play a role for the player-instrument interaction. Especially a film sensor at the frog – with some modifications to the present design – could be an appropriate tool to access the available vibrotactile input. The vibrations felt with the bowing hand at the frog are also potentially relevant for judging the quality of the bow and even of the instrument, similar to the vibrations at the left hand [33].

Acknowledgements

The authors would like to thank Frank Spahn for helpful discussions and Dmitry Rychkov for valuable advice.

References

[1] R. T. Schumacher: Some aspects of the bow. Catgut Acoustical Society Newsletter **24** (1975) 5–8.

[2] A. Askenfelt: Observations on the violin bow and the interaction with the string. Speech Transmission Laboratory, Stockholm: Quarterly Progress and Status Report **36** (1995) 107–118.

[3] C. E. Gough: Violin bow vibrations. The Journal of the Acoustical Society of America **131** (2012) 4152–4163.

[4] K. Guettler, A. Askenfelt: Relation between bow resonances and the spectrum of a bowed string. Proc. International Symposium of Music Acoustics, 1995, 231–237.

[5] R. Pitteroff, J. Woodhouse: Mechanics of the contact area between a violin bow and a string. Part I: Reflection and transmission behaviour. Acta Acustica united with Acustica **84** (1998) 543–562.

[6] A. Askenfelt: Observations on the dynamic properties of violin bows. STL-QPSR **33** (1992) 43–49.

Document downloaded by @DAEL, 2026-11-26 14:50:23 - personal use only

[7] C. E. Gough: The theory of string resonances on musical instruments. Acta Acustica united with Acustica **49** (1981) 124–141.

[8] G. Weinreich: Coupled piano strings. The Journal of the Acoustical Society of America **62** (1977) 1474–1484.

[9] G. Bissinger, K. Ye: Effect of holding on the normal modes of an instrumented violin bow. Proc. 17th Intern. Modal Analysis Conf.–Soc. Exp. Mechanics, 1999, 126–130.

[10] A. Askenfelt: Measurement of the bowing parameters in violin playing. II: Bow–bridge distance, dynamic range, and limits of bow force. The Journal of the Acoustical Society of America **86** (1989) 503–516.

[11] M. Demoucron, A. Askenfelt, R. Caussé: Measuring bow force in bowed string performance: Theory and implementation of a bow force sensor. Acta Acustica united with Acustica **95** (2009) 718–732.

[12] E. Maestre: Analysis/synthesis of bowing control applied to violin sound rendering via physical models. Proceedings of Meetings on Acoustics ICA2013, 2013, 035016.

[13] N. H. Rasamimanana, E. Fléty, F. Bevilacqua: Gesture analysis of violin bow strokes. International Gesture Workshop, 2005, Springer-Verlag Berlin Heidelberg, 145–155.

[14] E. Schoonderwaldt, K. Guettler, A. Askenfelt: An empirical investigation of bow-force limits in the Schelleng diagram. Acta Acustica united with Acustica **94** (2008) 604–622.

[15] D. S. Young: A methodology for investigation of bowed string performance through measurement of violin bowing technique. Dissertation. Massachusetts Institute of Technology, 2007.

[16] C. V. Raman: On the mechanical theory of the vibrations of bowed strings and of musical instruments of the violin family, with experimental verification of the results. Part I. Bulletin of the Indian Association for the Cultivation of Science **15** (1918) 1–158.

[17] J. C. Schelleng: The bowed string and the player. The Journal of the Acoustical Society of America **53** (1973) 26–41.

[18] J. Woodhouse: On the playability of violins. Part II: Minimum bow force and transients. Acta Acustica united with Acustica **78** (1993) 137–153.

[19] K. Guettler: On the creation of the Helmholtz motion in bowed strings. Acta Acustica united with Acustica **88** (2002) 970–985.

[20] H. Mansour, J. Woodhouse, G. Scavone: Time-domain simulation of the bowed cello string: Dual-polarization effect. Proceedings of Meetings on Acoustics, 2013, Acoustical Society of America, 035014.

[21] P. M. Galluzzo, J. Woodhouse: High-performance bowing machine tests of bowed-string transients. Acta Acustica united with Acustica **100** (2014) 139–153.

[22] R. Mores: Maximum bow force revisited. The Journal of the Acoustical Society of America **140** (2016) 1162–1171.

[23] R. Gerhard: A matter of attraction: Electric charges localised on dielectric polymers enable electromechanical transduction. 2014 IEEE Conference on Electrical Insulation and Dielectric Phenomena (CEIDP), 2014, IEEE, 1–10.

[24] R. Gerhard, S. Bauer, X. Qiu: Charge-spring model for predicting the piezoelectric response of dielectric materials: Considering tetragonality extends validity to ferroelectric crystals. 2016 IEEE Conference on Electrical Insulation and Dielectric Phenomena (CEIDP), 2016, IEEE, 81–84.

[25] M. Wegener, S. Bergweiler, D. Zscherpel, W. Wirges, R. Gerhard(-Multhaupt): Detection of elliptical oscillations and monopole breathing of organ-pipe bodies with piezoelectric polymer sensors. Acta Acustica united with Acustica **92** (2006) 476–481.

[26] M. Kappel: Scattering effects in the sound wave propagation of instrument soundboards. Dissertation. University of Potsdam, 2012.

[27] G. Gidion, R. Gerhard: Characterization of bridge motions on the violin using polymer sensor technology. Proceedings of Meetings on Acoustics, 2013, Acoustical Society of America, 035005.

[28] M. Wegener, W. Wirges, J. Fohlmeister, B. Tiersch, R. Gerhard(-Multhaupt): Two-step inflation of cellular polypropylene films: void-thickness increase and enhanced electromechanical properties. Journal of Physics D: Applied Physics **37** (2004) 623.

[29] X. Qiu, L. Holländer, W. Wirges, R. Gerhard, H. C. Basso: Direct hysteresis measurements on ferroelectret films by means of a modified Sawyer–Tower circuit. Journal of Applied Physics **113** (2013) 224106.

[30] F. Ablitzer, J.-P. Dalmont, N. Dauchez: Static model of a violin bow: influence of camber and hair tension on mechanical behavior. The Journal of the Acoustical Society of America **131** (2012) 773–782.

[31] L. Cremer: Physik der Geige. Hirzel Stuttgart, 1981.

[32] M. Möser, W. Kropp: Körperschall. Springer-Verlag, 2010.

[33] C. Fritz, J. Poitevineau, S. McAdams: Investigating the role of auditory and tactile modalities in violin quality evaluation. PloS one **9** (2014) e112552.

Document downloaded by @DAEL, 2026-11-26 14:50:23 - personal use only